A&A 480, 677–685 (2008)
DOI: 10.1051/0004-6361:20078799

Astronomy & Astrophysics

Anomalous X-ray emission in GRB 060904B: a nickel line?

R. Margutti[1,2], A. Moretti[2], F. Pasotti[2], S. Campana[2], G. Chincarini[1,2], S. Covino[2], C. Guidorzi[1,2], P. Mazzali[3,4,5,6], P. Romano[1,2], and G. Tagliaferri[2]

[1] Universitá degli Studi di Milano-Bicocca, Dipartimento di Fisica, Piazza della Scienza 3, 20126 Milano, Italy
e-mail: raffaella.margutti@brera.inaf.it
[2] INAF - Osservatorio Astronomico di Brera, via E. Bianchi 46, 23807, Merate (LC), Italy
[3] Max-Planck Institut für Astrophysik, Karl-Schwarzschild Str. 1, 85748 Garching, Germany
[4] Department of Astronomy, School of Science, University of Tokyo, Bunkyo-ku, Tokyo 113-0033, Japan
[5] Research Center for the Early Universe, School of Science, University of Tokyo, Bunkyo-ku, Tokyo 113-0033, Japan
[6] Istituto Nazionale di Astrofisica, Trieste Astronomical Observatory, Via G.B. Tiepolo 11, 34143 Trieste, Italy

Received 5 October 2007 / Accepted 30 November 2007

ABSTRACT

Context. The detection of an extra component in the GRB 060904B X-ray spectra in addition to the standard single power-law behaviour has recently been reported in the literature. This component can be fit with different models; the addition of a spectral line provides the best correspondence.
Aims. We investigate the physical properties that the surrounding medium must have in order to produce a spectral feature that can explain the detected emission.
Methods. We analyse and discuss how and if the detected spectral excess fits in different theoretical models developed to explain the nature of line emission during the afterglow phase of Gamma-Ray Bursts (GRBs). Transmission and reflection models have been considered.
Results. Given the high value ($\gg$1) of the Thomson optical depth, the emission is likely to arise in a reflection scenario. Within reflection models, the external reflection geometry fails to predict the observed luminosity. On the contrary, the detected feature can be explained in a funnel scenario with typical opening angle $\theta \sim 5°$, nickel mass $\sim$0.1 $M_{\odot}$ and $T = 10^6$ K. For $\theta \sim 20°$, assuming the reprocessing material to be in the SN shell, the detected emission implies a nickel mass $\sim$0.4 $M_{\odot}$ at $T \sim 10^7$ K and a metallicity $\sim$10 times the solar value. If the giant X-ray flare that dominates the early XRT light curve is identified as the ionizing source, the SN expansion began $\sim$3000 s before the GRB event.

Key words. gamma rays: bursts

1. Introduction

A direct observation of Gamma-Ray Burst (GRB) central engines is not possible; however, it is possible to infer something about the nature of their progenitors if indirect probes of the physical conditions, structure and composition of the material at the GRB site can be found. X-ray spectroscopy is one probe.

The majority of X-ray spectra of afterglows detected by Swift show a power law behaviour, (see e.g. O'Brien et al. 2006) the result of non thermal emission, the leading candidate for which is syncrotron emission (Piran 2005, and references therein). Any deviation from this standard behaviour would require investigation.

Detections of emission and absorption features in addition to the basic absorbed power law have been claimed in a number of observations (see Sako et al. 2005, their Table 2 for a comprehensive summary). Most are interpreted as Fe Kα emission. The emission line radiation is supposed to be produced through reprocessing of the burst radiation: for this reason its luminosity, spectral shape and wavelength shift carry important information not only about the geometry and structure of the surrounding medium, but also about the physical conditions at the GRB site and the same GRB energetics (Ghisellini et al. 2002). However, the statistical significance of the claimed detections has been questioned by Sako et al. (2005): a large fraction of the claims are based on using the F-test, a statistical method that gives both false positives and false negatives when applied to emission or absorption features (Protassov et al. 2002). After a re-analysis of the data based on Monte Carlo simulations, Sako et al. (2005) ruled out all of the reported features.

Recently, new detections have been claimed by Butler (2007) and Moretti et al. (2007, hereafter M07). In particular, M07 focused on spectra of GRBs with know redshift detected by Swift in the period April 2005–January 2007 with very steep spectra (photon index $\Gamma > 3$, value obtained with an absorbed single power law – hereafter SPL – fit). Out of 13 spectra with more than 2000 photons satisfying this condition, highly significant deviations from the SPL spectral model have been found in 4 cases. These spectra belong to GRB 060502A, GRB 060729, GRB 060904B and GRB 061110A. These bursts were detected by *Swift*. In one case (GRB 060904B) the excess can be modeled by the emission line of highly ionized nickel (see Fig. 1).

We refer the reader to M07 for details about the sample selection and the statistical methods used.

In this paper we analyse and discuss how and if the spectral excess detected in GRB 060904B fits in the different models developed to explain the production of line emission during the afterglow phase of GRBs. In particular, the theoretical implications of the possible detection of nickel emission $\approx$200 s (see Fig. 2) after the onset of the GRB event are explored.

This paper is organised as follows: the spectroscopic identification of the line emission is discussed in Sect. 2. In the same

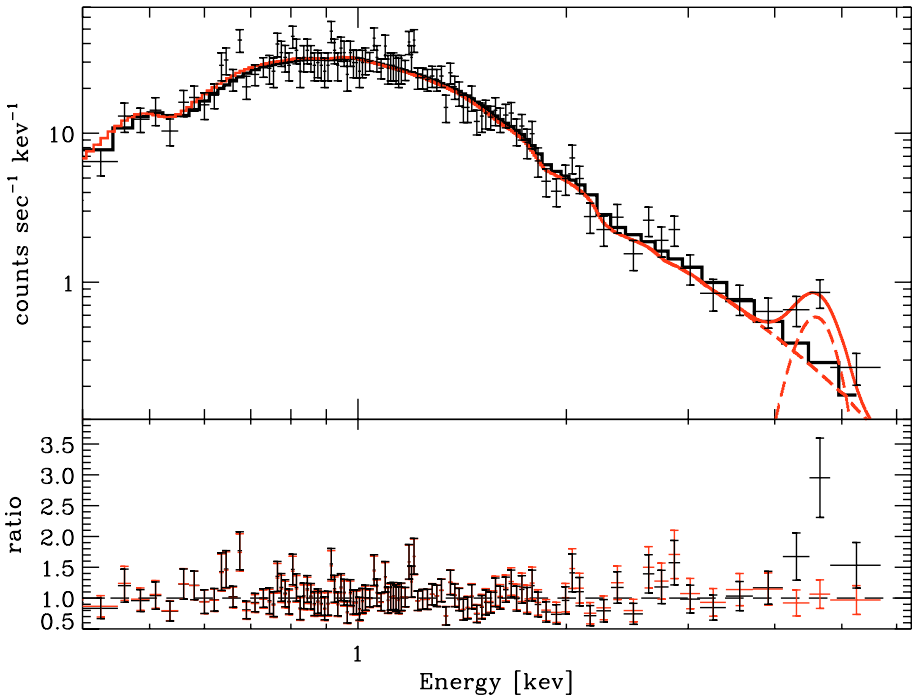

Fig. 1. *Upper panel*: GRB 060904B spectrum observed in the rest frame time interval 138−185 s. Solid thick black line: best fit absorbed simple power-law model (SPL): photon index $\Gamma = 3.55^{+0.08}_{-0.08}$; neutral absorber column density at the source redshift $N_{\rm H,z} = (0.69^{+0.04}_{-0.04}) \times 10^{22}$ cm^{-2}. Thin coloured line: best fit absorbed power-law plus Gaussian model (GAU): $\Gamma = 3.67^{+0.10}_{-0.09}$; $N_{\rm H,z} = (0.74^{+0.05}_{-0.05}) \times 10^{22}$ cm^{-2}; the values of the parameters related to the Gaussian component are reported in Table 1. The Galactic hydrogen column density $N_{\rm H,MW}$ is fixed to the value reported in Dickey & Lockman (1990) along the GRB direction (M07). *Lower panel*: ratio between the observed values and the model predicted values (in color in the online edition).

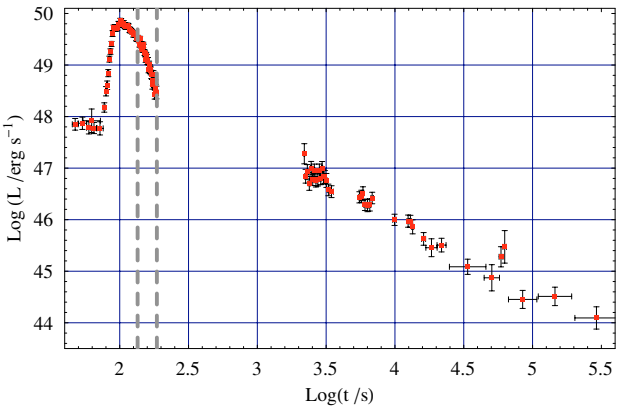

Fig. 2. Luminosity curve of GRB 060904B in the observed 0.3−10 keV energy band (XRT observations). Rest frame times as measured from the BAT trigger have been used. Grey dashed lines: interval of time during which the anomalous emission arises.

Table 1. Best fit parameters and physical quantities related to the spectral excess detected in the GRB 060904B X-ray afterglow. The spectrum has been modeled with an SPL with a Gaussian component superimposed to fit the line profile: time interval between the GRB explosion (BAT trigger) and the detection of the spectral excess; observed duration of the anomalous emission; Gaussian width; Gaussian central energy; luminosity of the additional spectral component; equivalent width. Rest frame values are provided (from M07).

$t_{\rm det}$	138	(s)
Δt^a	47	(s)
σ_ν	$0.50^{+0.35}_{-0.17}$	(keV)
E_0	$7.85^{+0.16}_{-0.25}$	(keV)
$L_{\rm line}$	1.10 ± 0.18	(10^{47} erg/s)
EW	2.0 ± 0.3	(keV)

Lower limit to the real duration of the emission because of a gap of observation between ∼200 s and ∼2000 s (rest frame values) after the GRB onset. Hence we can write 47 s $\leq \Delta t <$ 2000 s.

section. we derive simple constraints to the theoretical models starting from purely geometrical considerations. We discuss the relevant physical quantities linked to the detected emission in Sect. 3. Theoretical models are derived in Sect. 4. We address the problem of the ionizing source in Sect. 5, while in Sect. 6 we derive limits to the GRB total energy reservoir starting from the detected line luminosity. Our results are discussed in Sect. 7. Conclusions are drawn in Sect. 8.

The data reduction and temporal analysis have been performed using the standard HEADAS software, v6.1; for the spectral analysis we used XSPEC (v11.3). Unless otherwise stated, we quote errors at the 68% confidence level. Throughout this paper a standard concordance cosmology is used: $\Omega_{\rm m} = 0.27$, $\Omega_\Lambda = 0.73$, $h_0 = 0.71$.

2. Spectroscopic identification and geometric constraints

For GRB 060904B, the statistically significant deviation from the SPL spectral model is best modeled by an additional Gaussian component (see Fig. 1). After a Monte Carlo analysis, M07 report a multitrial significance of the excess greater that 99.9%. We refer the reader to M07 for details. Table 1 shows the physical quantities related to the detected excess. Unless otherwise stated, rest frame values are used (the burst is located at $z = 0.703$; Fugazza et al. 2006).

The detected excess is centered at 7.85 keV in agreement with what we expect from highly ionised nickel line emission: the k_α emission of H-like (He-like) nickel is expected to

lie at 8.10 keV (7.81 keV). Such detection differs from previous claims of line emission in GRB afterglows because of the much higher luminosity involved (about 3 orders of magnitude higher; see e.g. Böttcher 2004, and references therein), and because of the short delay between the GRB event and the line detection ($\approx 10^2$ s). In previous claims of line detection, the event has been reported to occur at later times, i.e. 10^4–10^5 s after the GRB detection.

The link between GRB events and supernova (SN) explosions has been established in a number of observations (see e.g. Galama et al. 1998; Stanek et al. 2003; Malesani et al. 2004; Campana et al. 2006). *If* we require the line emitting material to be the SN shell, then from the failed detection of Co features at a 3σ confidence level we derive an upper limit to the remnant age: $t_{\rm remn} \leq 6$ days. (The time evolution of Ni, Co and Fe abundances as modeled by Woosley & Weaver 1995 has been assumed). Adopting $v_{\rm shell} \approx 10^9$ cm s^{-1} as a typical expansion velocity of the SN shell at early stages (see e.g. Patat et al. 2001), the maximum distance travelled by the reprocessing material is therefore $R_{\rm max} \approx 10^{15}$ cm. Assuming a contemporaneous SN-GRB explosion this distance shrinks to $\approx 4 \times 10^{12}$ cm. On the other hand, from purely geometrical considerations the detection of the line emission at $t_{\rm det}$ requires the material to be located within a distance $R = c\, t_{\rm det}(1-\cos\phi)^{-1} \approx 4 \times 10^{12} (t_{\rm det}/138\,{\rm s})(1-\cos\phi)^{-1}$ cm. Note that $R \geq 10^{16}$ cm only for $\phi \leq 1^\circ$, where ϕ is the angle between the line emitting material and the line of sight at the GRB site. For these reasons we consider unlikely the possibility that the detected line emission originates from a distant ($R \geq 10^{16}$ cm) reprocessor scenario and we prefer nearby ($R \leq 10^{13}$ cm) reprocessor models. In such models the duration of the line emission is primarily linked to the time for which the central engine is active. Unfortunately we have only a poor lower limit to this parameter ($\Delta t \geq 47$ s) so that geometric factors can also be an important contributor to the observed line duration. (In the first $\approx$130 s the high level of continuum emission prevents us from detecting any spectral feature with the same luminosity even if present, while no data were collected by *Swift* between ~200 s and ~2000 s after the onset of GRB 060904B.)

3. Physical conditions

Emission time scale – A line photon is produced each time an electron recombines. The time scale of the emission process is therefore set by the slowest of the ionization and the recombination processes. Even under the assumption of a ionizing luminosity similar to the luminosity of the observed excess, it can be shown that $t_{\rm ion} \ll t_{\rm rec}$, so that the ionization is essentially istantaneous. The observed line luminosity implies an emission rate of nickel line photons of $\dot{N} = L_{\rm line}/\epsilon_{\rm Ni} \approx 10^{55}$ s^{-1} ($\epsilon_{\rm Ni} \approx 8$ keV); if each nickel atom recombines only once, then the emitting nickel mass is given by $M_{\rm Ni} = 56 m_{\rm p} \dot{N} \Delta t \approx 20\ M_\odot$[1]. However, nickel masses as large as $\approx 20\ M_\odot$ are difficult to account for in any reasonable physical scenario. We therefore conclude that each nickel atom recombines more than once in $\Delta t \approx 47$ s, or $t_{\rm rec} < 47$ s. Using the expression of the recombination time of a hydrogenic ion of atomic number $Z = 28$ given by Verner & Ferland (1996) the previous expression turns into a condition on the electron density and temperature of the plasma. The allowed parameter space is shown in Fig. 3.

[1] Note that in this paper we refer to ^{56}Ni since this is the Ni isotope most produced during SN explosions.

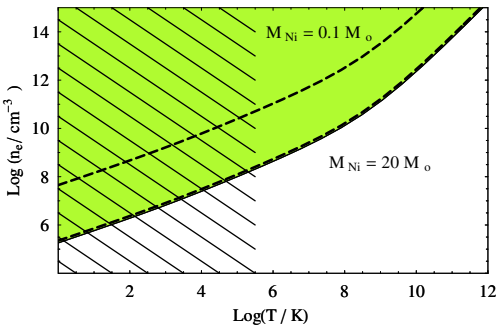

Fig. 3. Coloured area: electron number density-temperature parameter space valid for $t_{\rm rec} < 47$ s for GRB 060904B. The dashed lines mark the $0.1\ M_\odot < M_{\rm Ni} < 20\ M_\odot$ region, where $M_{\rm Ni}$ is the *emitting* nickel mass. The shaded area represents the $T \leq 3.2 \times 10^5$ K region. The electron temperature is likely to be higher than this value at this stage of the SN explosion (Arnett 1996).

Thomson optical depth – The Thomson optical depth of the SN shell of radius R and total mass M is given by:

$$\tau_{\rm T} \sim \frac{1}{\mu_{\rm e} m_{\rm p}} \frac{\sigma_{\rm T}}{4\pi R^2} \left(\frac{M_{\rm Ni^*}}{X}\right) \quad (1)$$

where $\mu_{\rm e}$ is the mean molecular weight; $X = M_{\rm Ni^*}/M$; $M_{\rm Ni^*}$ is the *total* Ni mass. The photoionization optical depth for He-like or H-like nickel can be written as:

$$\tau_{\rm Ni} = \frac{\xi\, \sigma_{\rm Ni}}{\sigma_{\rm T}} \frac{X \mu_{\rm e}}{56}\, \tau_{\rm T} \quad (2)$$

where ξ is the ionised to total nickel abundance ratio and $\sigma_{\rm Ni}$ is the He-like or H-like nickel photoionization cross section ($\approx 10^{-20}$ cm^{-2}, from Verner & Yakovlev 1995). It is easy to show that $\tau_{\rm T} \gg 1$ for $R \sim 10^{12}$–10^{13} cm and $M > 10^{-5}\ M_\odot$, where M is the total mass of the remnant shell. While an efficient use of the H-like or the He-like nickel ions requires $\tau_{\rm Ni} \geq 1$, a Thompson optical depth larger than one is a problem: if photons diffuse through a plasma cloud in which Thomson scattering is the predominant mechanism and if the cloud has a central photon source, then the average number of scatterings experienced by a photon will be $\approx 1/2\, \tau_{\rm T}^2$ (see e.g. Sunyaev & Titarchuk 1980). With $\tau_{\rm T} \gg 1$, the line would be smeared in the continuum and no detection would be possible. We must therefore require the line photons not to have crossed such regions along our line of sight. This in turn implies that the electron clouds are not isotropically distributed around the GRB location, in order to allow the line photons to freely escape. A $\tau_{\rm T} \gg 1$ favours models in which the line is produced by reflection; in this case line photons come from the thin layer of material with $\tau_{\rm Ni} \approx$ several or $\tau_{\rm T} \leq 1$. Trasmission models instead require the emitting material to *globally* have $\tau_{\rm T} \leq 1$.

Line width – We consider the different physical processes that could lead to the observed line broadening ($\approx$0.5 keV, Table 1). A purely thermal broadening requires $T \approx 10^{12}$ K, a temperature that is difficult to account for in any reasonable physical scenario. At the same time this would also cause the recombination efficiency to drop. On the other hand, if the bulk expansion of the SN remnant is the source of the observed broadening, then a velocity of the emitting atoms $\approx 25\,000$ km s^{-1} is required. Such velocities are indeed observed during the firts stages of Hypernova (HN) explosions associated with GRB events (see e.g. Patat et al. 2001).

An alternative broadening mechanism is Compton scattering by free electrons of the emitting material. In high temperature

gas the first scattering will produce an average energy broadening $\Delta E/E \approx (2k_bT/m_ec^2)^{1/2}$ (Sunyaev & Titarchuk 1980). For the emission feature detected in GRB 060904B spectra, this directly translates into $T \approx 10^7$ K. It is however possible that the real electron temperature is lower and that line photons undergo numerous scatterings before reaching the observer. In this case the centroid of the line would be redshifted (line photons are mostly backscattered by colder electrons) with an average energy shift given by $\Delta E \approx 0.12\, N_{sc}^{1/2}$ keV, where the N_{sc} stands for the number of suffered scatterings (Sunyaev & Titarchuk 1980). At the same time the multiple scattering process would further smear the line out, making it more difficult to detect. It is therefore reasonable that $N_{sc} \sim$ a few.

Given the poor statistics, it is not possible to discuss in detail the line profile. In the following, results will be discussed for electron temperatures in the range 10^6–10^8 K.

4. The models

In this section we discuss models in which the line is due to reflection (see Sect. 3). The underlying physical mechanism is fast ionizations and recombinations.

Reflection models (see Böttcher 2004, for a review) require the presence of a dense optically thick medium surrounding the burst site. Moreover, an anisotropic distribution of the material is required in order to have a clean path where line photons can propagate and reach the observer without being smeared in the continuum (see Fig. 4). The ionizing flux is efficiently reprocessed in line photons in a superficial layer of the material with $\tau_T \sim 1$ (in order to avoid excessive Compton broadening) and $\tau_{Ni} \sim$ several, to efficiently reprocess the continuum radiation. The volume V_{em} effectively contributing to the observed line emission is therefore given by $V_{em} \approx S\,\Delta R$ or $V_{em} \approx S/\sigma_T n_e$. The line luminosity can be expressed as:

$$L_{line} = \frac{n_{Ni} V_{em} \epsilon_{Ni}}{t_{rec}} = \frac{n_{Ni} S\, \epsilon_{Ni} \alpha_r(Z,T)}{\sigma_T} \tag{3}$$

where:

σ_T : Thomson cross section;
n_e : electron number density;
n_{Ni} : Ni number density;
S : emitting surface;
ϵ_{Ni} : energy of a single line photon (≈8 keV);
$\alpha_r(Z,T)$: recombination coefficient as a function of the atomic number Z and temperature T (from Verner & Ferland 1996). $[\alpha_r] = \mathrm{cm}^3/\mathrm{s}$.

In the following, two alternative geometries of emission will be considered: an external reflection geometry and a stratificated funnel geometry (Vietri et al. 2001).

4.1. External reflection model

According to the external reflection model, the line emitting material is back-illuminated by burst or afterglow photons scattered by preburst stellar wind (we refer the reader to Vietri et al. 2001, and references therein for details). In this model the line emitting material has been ejected at subrelativistic speeds along the progenitor equator in a simultaneous SN-GRB explosion. The luminosity L_{scatt} back-scattered by electrons moving outward from the source is of the order of (Vietri et al. 2001):

$$L_{scatt} \approx 1.8 \times 10^{45} \frac{\dot{m}_{w,-5}}{v_{w,7}}\ \mathrm{erg\ s^{-1}} \tag{4}$$

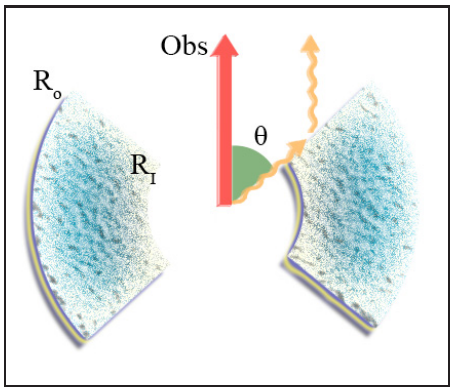

Fig. 4. Geometry assumed for the reflecting material for the funnel model discussed in the text.

where $\dot{m}_{w,-5} = \dot{m}_w/(10^{-5}\ M_\odot\ \mathrm{yr}^{-1})$ and the symbol $\dot{m}_w$ stands for the progenitor mass loss rate; $v_{w,7} = v_w/(10^7\ \mathrm{cm\ s}^{-1})$, v_w being the wind velocity. This is already 2 orders of magnitude *lower* than the observed line luminosity and ≈4 orders of magnitude lower than the expected ionizing luminosity: Lazzati et al. (2002) show that in optimal conditions a reprocessing efficiency of ≈1% at most can be reached, so that for the emission feature detected in GRB 060904B $L_{ion} \geq 10^{49}$ erg s^{-1} is required. A fine-tuning of the progenitor wind velocity and of the mass-loss rate is therefore required to explain the observed line luminosity. For this reason we consider this scenario unlikely.

4.2. Funnel model

In this model the line emitting material is provided by the walls of a funnel excavated in a young SN shell (Lazzati 2000). A cone geometry of opening angle θ is assumed for simplicity (see Fig. 4). Considering a power-law electron number density profile:

$$n_e = n_I \left(\frac{r}{R_I}\right)^{-\alpha} \tag{5}$$

Eq. (3) translates into:

$$L_{line} = \frac{\mu_e X}{56\sigma_T} \epsilon_{Ni}\, 2\pi\, \alpha_r(Z,T) \sin(\theta) n_I R_I^\alpha \int_{R_I}^{R_o} r^{1-\alpha}\, dr \tag{6}$$

where:

$$n_{Ni} = n_e \frac{\mu_e X}{56} = \frac{n_e \mu_e}{56} \frac{M^*_{Ni}}{M}\,. \tag{7}$$

The total[2] Ni mass M^*_{Ni} can be written as:

$$M^*_{Ni} = X\, M = X \left(4\pi \mu_e m_p \cos(\theta) n_I R_I^\alpha \int_{R_I}^{R_o} r^{2-\alpha}\, dr\right) \tag{8}$$

where m_p is the proton mass. This allows us to derive the line luminosity independently of the quantity $n_I R_I^\alpha$:

$$L_{line} = M^*_{Ni} \frac{\epsilon_{Ni}\, \alpha_r(Z,T)}{112\sigma_T m_p} \tan(\theta) \frac{\int_{R_I}^{R_o} r^{1-\alpha} dr}{\int_{R_I}^{R_o} r^{2-\alpha} dr}\,. \tag{9}$$

[2] The fraction of the total Ni mass actually contributing to the detected emission is indicated by M_{Ni}.

The previous relation assumes $t_{\rm rec} > t_{\rm ion}$. A rough estimate of the ionization time scale $t_{\rm ion}$ for material located at a distance R from the photon source of luminosity $L_{\rm ion}$ is given by:

$$t_{\rm ion} \approx \frac{\Omega R^2 \epsilon_{\rm ion}}{L_{\rm ion}\sigma_{\rm Ni}} \tag{10}$$

where $\epsilon_{\rm ion}$ is the energy of the ionizing photons; the parameter Ω allows for the possibility of collimated flux of ionizing photons. The recombination time scale can be written as:

$$t_{\rm rec} = \frac{1}{n_{\rm e}\alpha_{\rm r}(Z,T)}\,. \tag{11}$$

For the funnel cone geometry, the condition $t_{\rm rec} > t_{\rm ion}$ therefore becomes:

$$\frac{t_{\rm rec}}{t_{\rm ion}} = \frac{L_{\rm ion}\sigma_{\rm Ni}}{\Omega\epsilon_{\rm ion}\alpha_{\rm r}(Z,T)}\frac{1}{n_{\rm I}R_{\rm I}^{\alpha}\,r^{2-\alpha}} > 1. \tag{12}$$

As before, inserting $n_{\rm I}R_{\rm I}^{\alpha}$ from Eq. (8) and assuming the collimation angle of the ionizing photons to be $\sim\theta$ we finally derive:

$$\frac{t_{\rm rec}}{t_{\rm ion}} = \left(\frac{L_{\rm ion}\sigma_{\rm Ni}}{\epsilon_{\rm ion}\alpha_{\rm r}}\frac{2\cos(\theta)}{(1-\cos(\theta))}\frac{\mu_{\rm e}m_{\rm p}}{M}\frac{1}{r^{2-\alpha}}\int_{R_{\rm I}}^{R_{\rm o}} r^{2-\alpha}\,{\rm d}r\right) > 1. \tag{13}$$

The system of equations that defines the funnel model is therefore:

$$\begin{cases} L_{\rm line} = M^{*}_{\rm Ni}\frac{\epsilon_{\rm Ni}\,\alpha_r(Z,T)}{112\sigma_{\rm T}m_{\rm p}}\tan(\theta)\frac{\int_{R_{\rm I}}^{R_{\rm o}} r^{1-\alpha}{\rm d}r}{\int_{R_{\rm I}}^{R_{\rm o}} r^{2-\alpha}{\rm d}r} \\ \frac{L_{\rm ion}\sigma_{\rm Ni}}{\epsilon_{\rm ion}\alpha_{\rm r}}\frac{2\cos(\theta)}{(1-\cos(\theta))}\frac{\mu_{\rm e}m_{\rm p}}{M}\frac{1}{r^{2-\alpha}}\int_{R_{\rm I}}^{R_{\rm o}} r^{2-\alpha}\,{\rm d}r > 1 \\ R_{\rm o} - R_{\rm I} \approx c\Delta t \end{cases} \tag{14}$$

where in the last equation the duration Δt of the line emission is required to be comparable with the time needed by the source photons to cross the SN shell. The observed or fixed quantities are the following:

- $L_{\rm line}$: line luminosity (1.10×10^{47} erg s^{-1});
- $\epsilon_{\rm ion}$: energy of the ionizing photons (the ionization threshold is ~10 keV);
- $\epsilon_{\rm Ni}$: energy of line photons (~8 keV)
- $R_{\rm I}$: internal radius of the shell, supposed to be comparable to the stellar progenitor radius. In order to reduce the parameter space, the system will be solved for $R_{\rm I} = 10^{11}$ cm (typical WR radius) and $R_{\rm I} = 10^{12}$ cm (typical blue supergiants radius).
- $L_{\rm ion}$: an efficiency of converting the illuminating continuum into the specific line of ~1% is assumed (Lazzati et al. 2002). For this reason the system will be solved for $L_{\rm ion} \sim 10^{49}$ erg s^{-1};
- $\mu_{\rm e}$: mean molecular weight. For a completely ionised material $\mu_{\rm e} = 1, 1.2$ and 2 for pure hydrogen, solar composition and no hydrogen respectively. In the following we assume $\mu_{\rm e} \approx 2$.

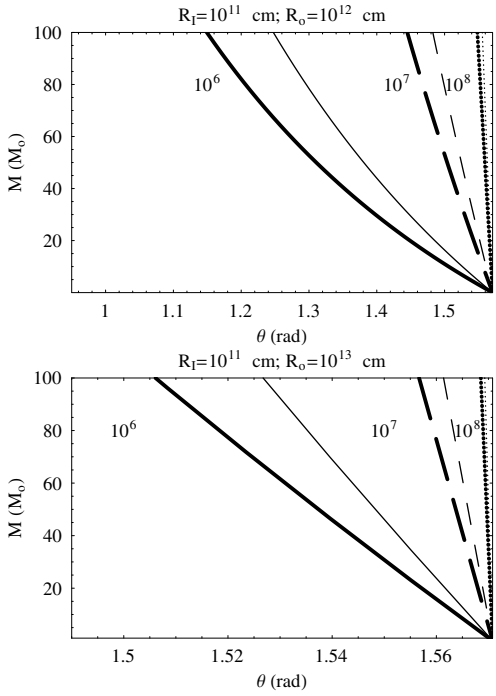

Fig. 5. Upper limits to the total mass of the shell derived from the second relation of the system 14 evaluated at $r = R_{\rm o}$ as a function of the funnel opening angle. Solid lines: $T = 10^6$ K; dashed lines: $T = 10^7$ K; dotted lines: $T = 10^8$ K. Thick lines: $\alpha = 0$; thin lines: $\alpha = 1$.

The unknown physical quantities of the system are:

- θ : Funnel opening angle;
- $M^{*}_{\rm Ni}$: total Ni mass. We expect $M^{*}_{\rm Ni} \leq 1\ M_{\odot}$ (see e.g. Arnett 1996). In particular, if the undetected SN associated with GRB 060904B is similar to other well studied SNe associated with GRB events, then $M^{*}_{\rm Ni} \sim 0.4\ M_{\odot}$ is expected (see e.g. Iwamoto et al. 1998; Mazzali et al. 2003; Mazzali et al. 2006b; Mazzali et al. 2006a). Results will be calculated for solar metallicity $X = 1.8 \times 10^{-3}$, $X = 1.8 \times 10^{-2}$ and $X = 1.8 \times 10^{-1}$;
- $R_{\rm o}$: outer radius of the shell. From the third relation of the Eq. (14) we expect $R_{\rm o} - R_{\rm I} \geq 10^{12}$ cm;
- α : mass density power-law index. The mass density of a SN shell can be approximated by a power-law in radius for radii greater than some critical value, while at radii less than critical the density is roughly constant. The critical radius evolves with time; its exact value is a function of the SN energy, the ejected mass and the density power law index. However, at early times from the SN explosion ($t < 1$ hr) the density profile is nearly constant within $R_{\rm o}$ (see e.g. Blondin & Ellison 2001). At this distance the density undergoes a rapid cutoff (see e.g. Arnett 1996, their Fig. 13.2). For this reason we will consider only small values of the power-law index: $0 \leq \alpha \leq 1$.

Our numerical results for the characteristic quantities of the problem are presented in Figs. 5–8. Figure 5 shows the variation of the upper limit to the total mass of the SN shell derived from the second relation of the system (14) as a function of the funnel opening angle. As the temperature rises, the recombination time increases, so that at a fixed funnel opening angle, more

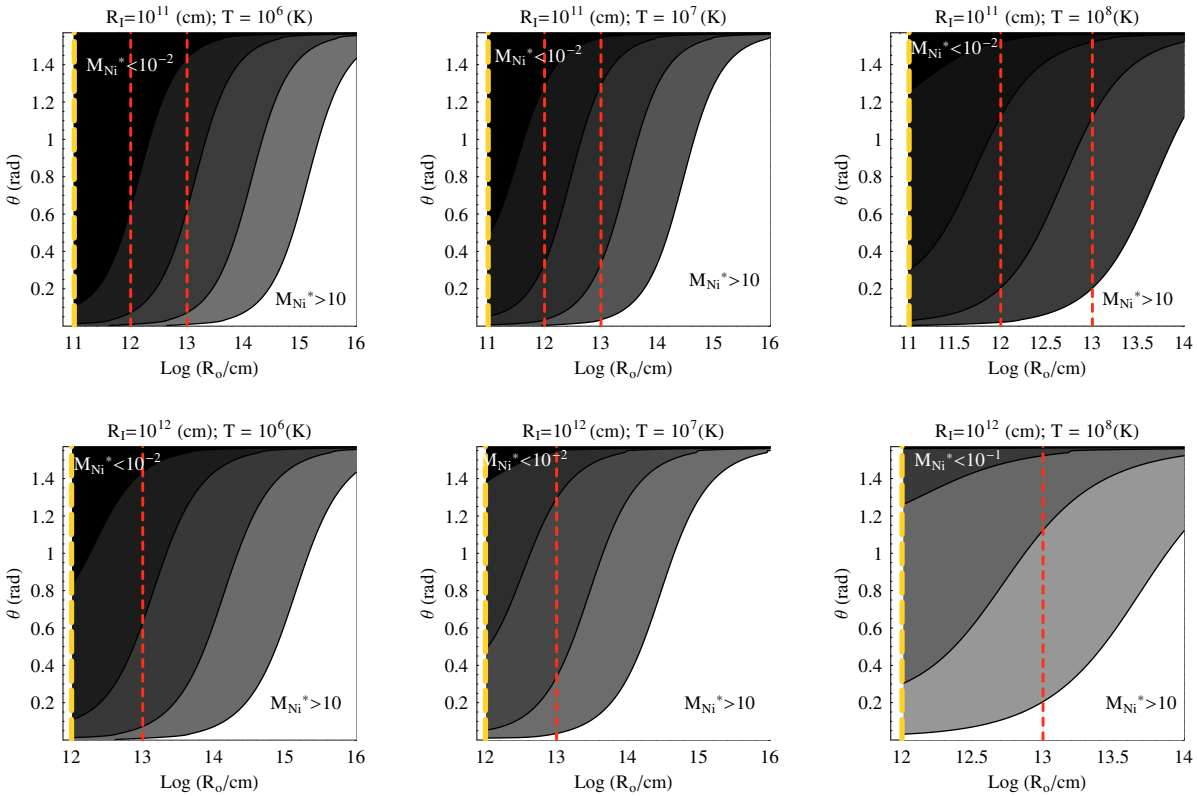

Fig. 6. Total Ni mass contour plot according to the first relation of the system (14) as a function of the funnel opening angle θ and the outer radius of the shell R_o. Results are shown for the different electron temperatures indicated, $R_I = 10^{11}$ cm and 10^{12} cm and $\alpha = 0$. In each plot, *from left to right*, the black solid lines mark the $M^*_{Ni} = 10^{-2}\ M_\odot$, $10^{-1}\ M_\odot$, $1\ M_\odot$ and $10\ M_\odot$ region. Red dashed lines: $R_o = 10^{12}$ cm and $R_o = 10^{13}$ cm. $L_{line} = 1.10 \times 10^{47}$ erg s^{-1}, $\epsilon_{Ni} = 8$ keV have been used.

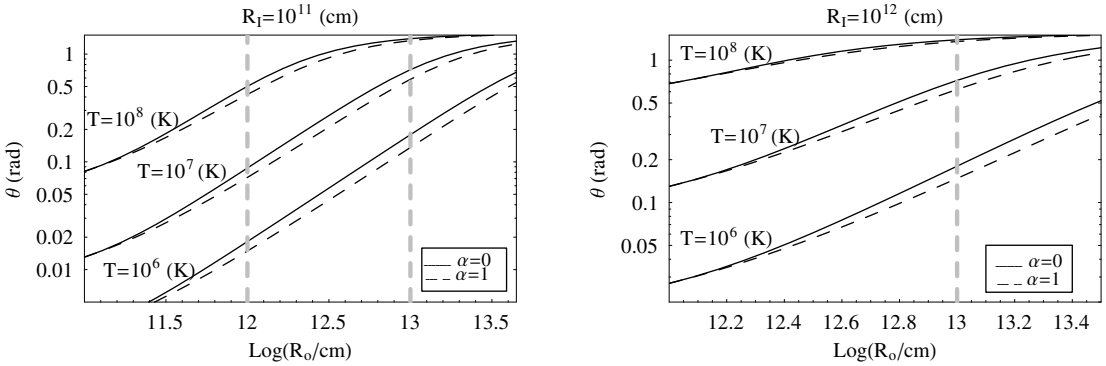

Fig. 7. Funnel opening angle (θ) versus outer shell radius (R_o) according to Eq. (14), first relation. A total Ni mass $M^*_{Ni} = 0.4\ M_\odot$ has been assumed (see the text for explanations). Results are shown for $R_I = 10^{11}$ cm (*left panel*) and $R_I = 10^{12}$ cm (*right panel*). In both panels the realtion is shown for three different temperatures: 10^6 K (*bottom*), 10^7 K and 10^8 K (*top*). Solid (dashed) black lines correspond to $\alpha = 0$ ($\alpha = 1$). Dashed grey lines: $R_o = 10^{12}, 10^{13}$ cm.

Ni is needed (and hence more mass in the SN shell) to fulfill the $t_{rec} = t_{ion}$ requirement. Consequently the condition $t_{rec} > t_{ion}$ will be satisfied by a more extended range of SN shell masses: for example, for $R_I = 10^{11}$ cm, $R_o = 10^{12}$ cm, $T = 10^7$ K we derive $M \leq 100\ M_\odot$ with $\theta \leq 1.45$ rad. For GRB-associated HNe, the ejected mass reported in the literature (see e.g. Iwamoto et al. 1998; Mazzali et al. 2003, 2006b,a) is however about one order of magnitude smaller. For this reason we expect $M \sim 10\ M_\odot$.

Figure 6 presents the variation of the total Ni mass required to explain the detected emission as a function of the funnel opening angle and the outer radius of the shell. Results are shown for different values of the internal radius and temperature. The stratification index has been fixed to 0. As the temperature rises, the required total Ni mass increases: this is due to the dependence of the recombination time on the temperature. On the other hand the increase of the funnel opening angle requires the detected emission to be explained by a smaller amount of Ni mass. This can be understood by considering that the density of the matter in the SN shell is a monotonic increasing function of θ. Consequently t_{rec} is a decreasing function of the funnel opening angle. The dependence of M^*_{Ni} on the matter density manifests itself also through the parameter R_o: the increase of the outer shell radius requires M^*_{Ni} to increase, in order to reproduce the luminosity of the detected emission feature. Finally, increasing R_I, M^*_{Ni} decreases.

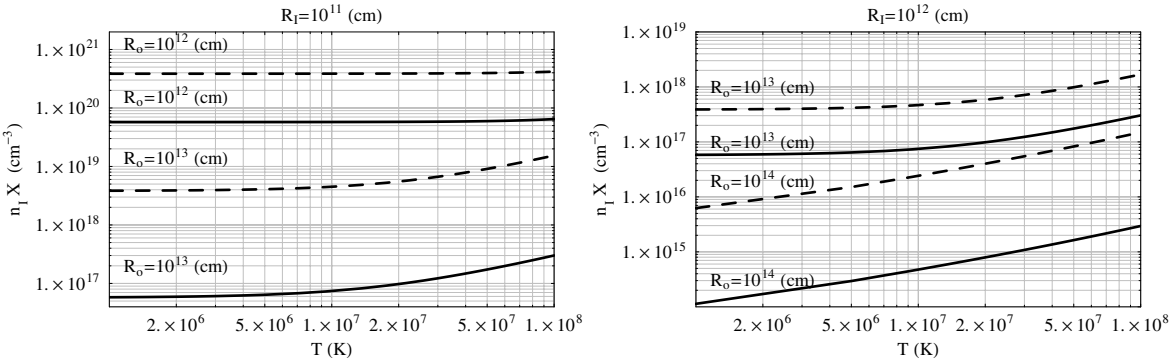

Fig. 8. Internal electron density $n_{\rm I}$ at the site of emission times the Ni abundance ratio $X = M^*_{\rm Ni}/M$ as a function of the temperature. A total Ni mass $M^*_{\rm Ni} = 0.4\ M_\odot$ has been assumed (see the text for explanations). *Left (right) panel*: $R_{\rm I} = 10^{11}$ cm ($R_{\rm I} = 10^{12}$ cm). In both panels results are shown for different values of the outer radius of the SN shell $R_{\rm o}$. Solid (dashed) lines: $\alpha = 0$ ($\alpha = 1$).

The dependence of the model on the value of the stratification index α is clear from Figs. 7 and 8: at a fixed outer radius, $\alpha = 1$ requires smaller values of the funnel opening angle and higher values of the internal electron density. While the θ–$R_{\rm o}$ relation is nearly insensitive to the variation of this parameter, as α increases from 0 to 1, the quantity $n_{\rm I}X$ increases by a factor $\approx 10^1$–10^2 (Fig. 8). Figure 7 shows the variations of the characteristic quantities of the problem assuming a total Ni mass of 0.4 $M_\odot$: for $T = 10^6$ K, $R_{\rm I} = 10^{11}$ cm, $R_{\rm o} = 10^{12}$ cm the model requires $\theta \approx 0.02$ rad ($\alpha = 0$). Increasing the electron temperature to 10^7 K (10^8 K) and keeping $\alpha = 0$, the opening angle increases to 0.08 rad (0.48 rad). The corresponding internal electron density at the emission site is $n_{\rm I} \approx 10^{20}$ cm^{-3}. The internal electron density would be about one order of magnitude lower if $\mu_{\rm e} \sim 16$, the value of the mean molecular weigth for a SN ejecta dominated by oxygen in a low ionization stage.

5. The ionizing source

The emission feature detected in GRB 060904B spectra is characterised by a large $EW = 2.0 \pm 0.3$ keV. Following Lazzati et al. (2002), we expect an underlying 1–10 keV continuum luminosity $L_{1-10\ \rm keV} \geq 100\ L_{\rm line}$ if this is to be identified with the ionizing source. From the *Swift* XRT light curve (see Fig. 2) we derive $L_{1-10\ \rm keV} = 4 \times 10^{48}$ erg s^{-1} at $t \sim 160$ s, the time at which we detect the emission feature. The *detected* underlying continuum is therefore *not* physically linked to the line emission.

The 1–10 keV rest frame luminosity as a function of time from the GRB onset is reported in Table 2. This table shows that the detected luminosity is actually higher than $100 L_{\rm line} \sim 10^{49}$ erg s^{-1} in the time interval 100–130 s. Assuming that the continuum illuminating the reprocessing material is similar to the observed radiation, it is possible to explain the detected emission feature requiring the ionizing emission to be isotropic and the reprocessing material to have a large covering factor. In this scenario the time delay between the arrival of direct continuum photons and the observation of the claimed line emission $\Delta t_{\rm D}$ is explained in terms of light travel time effects.

We assume that the ionizing photons are produced at $t \sim 100$ s after the GRB onset or at a travelled distance of $R \sim 3 \times 10^{12}$ cm. At this distance they interact with the SN material. An estimate of the funnel opening angle θ is therefore given by:

$$(R + R_{\rm p})\,\theta \sim c\Delta t_{\rm D} \tag{15}$$

where $R_{\rm p}$ is the progenitor radius. With $\Delta t_{\rm D} \sim 40$ s, the previous relation translates into $\theta \sim 22°$, 17° and 5° for $R_{\rm p} = 10^{11}, 10^{12}$ and 10^{13} cm. Moreover, assuming a typical expansion velocity $v_{\rm shell} \sim 10^9$ cm s^{-1}, we have:

$$v_{\rm shell}(t + t_{\rm SN}) \sim ct \tag{16}$$

where $t_{\rm SN}$ stands for the time delay between the GRB and the beginning of the SN expansion: for $t_{\rm SN} > 0$ the SN event happened before the GRB explosion. For $t \sim 100$ s the previous relation implies $t_{\rm SN} \sim 3000$ s.

Table 2. Rest frame isotropic 1–10 keV luminosity of GRB 060904B as a function of time from the GRB event. The XRT data have been split into different intervals of time, so that a minimum number of ≈2000 photons is containd in each spectrum. A SPL model has been assumed. Δt: interval of time; Γ: photon index (90% CI are listed); R: scale distance; n: particle density; ξ: ionization factor (see Sect. 7). For the interval of time containing the emission feature (point 7) only the SPL contribution has been reported.

	Δt	Γ	$L_{1-10\ \rm keV}$	$R^2 n$ $\xi = 10^4$
	(s)		(erg s^{-1})	(cm^{-1})
1	46–97	$1.61^{+0.11}_{-0.11}$	$8^{+0.4}_{-0.5} \times 10^{48}$	$8^{+0.4}_{-0.5} \times 10^{44}$
2	97–107	$1.93^{+0.11}_{-0.10}$	$4^{+0.2}_{-0.2} \times 10^{49}$	$4^{+0.2}_{-0.2} \times 10^{45}$
3	107–117	$2.36^{+0.15}_{-0.14}$	$3^{+0.2}_{-0.2} \times 10^{49}$	$3^{+0.2}_{-0.2} \times 10^{45}$
4	117–123	$2.56^{+0.12}_{-0.11}$	$2^{+0.1}_{-0.1} \times 10^{49}$	$2^{+0.1}_{-0.1} \times 10^{45}$
5	123–131	$2.81^{+0.12}_{-0.12}$	$2^{+0.1}_{-0.1} \times 10^{49}$	$2^{+0.1}_{-0.1} \times 10^{45}$
6	131–145	$3.15^{+0.15}_{-0.14}$	$1^{+0.1}_{-0.1} \times 10^{49}$	$1^{+0.1}_{-0.1} \times 10^{45}$
7	145–185	$3.75^{+0.19}_{-0.17}$	$4^{+0.2}_{-0.2} \times 10^{48}$	$4^{+0.2}_{-0.2} \times 10^{44}$
8	185–64 600	$2.22^{+0.15}_{-0.14}$	$2^{+0.2}_{-0.3} \times 10^{45}$	$2^{+0.2}_{-0.3} \times 10^{41}$

6. Limits on the total GRB energy

The emission feature detected in GRB 060904B shows an isotropic energy $E^{\rm iso}_{\rm line} \simeq L_{\rm line} \times \Delta t \geq 5 \times 10^{48}$ erg, where the inequality accounts for the lower limit we have on the duration of the emission. Following Ghisellini et al. (2002) the energy characterising the line emission can be used to set lower limits on the total energy reservoir of the GRB in the form of photons and kinetic energy:

$$E = \frac{E_\gamma}{\eta_\gamma} \geq 200 \frac{E^{\rm iso}_{\rm line}}{\eta_x \eta_\gamma} \frac{\Omega_{\rm line}}{4\pi} \tag{17}$$

where $\eta_{\rm x}$ is the bolometric corretion while the symbol η_γ stands for the efficiency in converting the kinetic energy into γ-rays.

A line efficiency of 1% has been assumed. For GRB 060904B this translates into:

$$E \geq 10^{53}\left(\frac{0.1}{\eta_x}\right)\left(\frac{0.1}{\eta_\gamma}\right) \text{ erg.} \quad (18)$$

No amplification factor $4\pi/\Omega_{\rm line}$ has been applied: from Sect. 5 $\theta \geq 5°$. Consequently, according to Ghisellini et al. (2002) the amplification factor due to electron scattering is ∼1. The derivation of a numerical value for the η_γ parameter depends on many physical parameters of the burst itself and its environment: in the conventional internal+external shock GRB model $\eta_\gamma \sim 1{-}5\%$ (Zhang & Mészáros 2004); however, allowing for an extremely inhomogeneous velocity of the ejecta shell $\eta_\gamma \sim 40\%$ (see Kobayashi et al. 1997; Kobayashi & Sari 2001). In a more recent study Zhang et al. (2007a) derive for 32 GRBs detected by *Swift* with early X-ray afterglow data $\eta_\gamma < 10\%$ at the end of the shallow decay phase; $\eta_\gamma > 90\%$ at the deceleration time of the fireball. The bolometric correction η_x is estimated using a Band spectrum (Band et al. 1993) with typical values of the parameters: we obtain $\eta_x \sim 0.1$.

From Eqs. (17) and (18) we derive $E_\gamma \sim 10^{52}(0.1/\eta_\gamma)$ erg. An independent estimate of the isotropic equivalent radiated energy $E_\gamma^{\rm iso}$ can be obtained as follows. Using the correlation between the SPL photon index Γ and the peak energy of GRB spectra measured by *Swift*-BAT in the energy band 15−150 keV (Zhang et al. 2007b) the photon index of 1.70 (Markwardt et al. 2006) translates into $E_{\rm p} \sim 85$ keV or $E_{\rm p,i} \sim 150$ keV (intrinsic peak energy). According to the Amati relation (Amati 2006), the isotropic equivalent radiated energy in the 1−10 000 keV cosmological rest frame is therefore $E_\gamma^{\rm iso} \sim 2 \times 10^{52}$ erg, in good agreement with the previous result.

Moreover, assuming the time interval during which the ionizing source has illuminated the reprocessing material to be comparable with the duration of the detected emission (the recombination time would be too small to account for the duration of the emission), we have $E_{\rm ill} \sim L_{\rm ion} \times \Delta t \geq 5 \times 10^{50}$ erg or $E_{\rm ill}^{\rm TOT} \sim 2\, L_{\rm ion} \times \Delta t \geq 10^{51}$ erg. The factor 2 in the previous relation has been added for geometrical reasons, since we expect a two-sided geometry with the line emitting material visible on only one side. For GRB 060904B this means that a fraction of the order of 1% of the radiated energy of the burst has illuminated the line emitting material.

7. Discussion

The XRT light curve of GRB 060904B is dominated by a giant flare in the first ≈200 s after the GRB onset (Fig. 2). At the end of this flare the spectrum becomes softer and an emission feature spectroscopically compatible with highly ionised Ni line emission arises.

The detected emission can be explained in a reflection scenario (Sect. 4). In these models high electron temperatures (≥10^9 K) require total masses of potentially line emitting material as high as ∼10 $M_\odot$ for $\theta \leq 60°$. This would in turn imply a mass of the shell remnant ≥100 $M_\odot$ even under the assumption of 100 times solar metallicity. For this reason, consistently with Sect. 3 we consider unlikely the $T \geq 10^9$ K scenario. If the funnel opening angle θ is to be identified with the jet opening angle θ_j, then $\theta \sim 60°$ at $t \sim 10^2$ s after the GRB onset is difficult to justify: Lamb et al. (2005), starting from theoretical considerations, concluded that GRBs have $\theta_j \sim 1°$; from the observational point of view, a typical $\theta_j \sim 5°$ is derived from the afterglow jet break data (Zhang et al. 2004). If $\theta \sim 5°$ (∼0.1 rad) the detected emission implies a total Ni mass of the order of 0.1 $M_\odot$ for $R_{\rm I} = 10^{11}$ cm, $R_{\rm o} = 10^{12}$ cm and $M_{\rm Ni}^* \geq 1\ M_\odot$ for $R_{\rm o} = 10^{13}$ cm, with $M_{\rm Ni^*}$ increasing from $T = 10^6$ to 10^7 K. Such high values of Ni mass suggest that the line emitting material is a SN remnant. (Note that up to this point no ad hoc assumption about the presence of the SN event has been made.) The same conclusion is reached using $R_{\rm I} = 10^{12}$ cm: in this case $\theta \sim 0.1$ rad favours $T \sim 10^6$ K (see Figs. 6 and 7). In this scenario the giant flare that dominates the early XRT ligth curve can not be identified with the ionizing source: in Sect. 5 we derived $\theta \geq 5°$. An undetected ionization source is therefore required. Alternatively, non geometrical factors must be invoked to explain the delay between the arrival of direct continuum photons and line photons.

However, in most cases *Swift* data do not support the existence of standard jet breaks: using high quality multi-wavelength data Covino et al. (2006) concluded that no convincing case of an achromatic break has been detected in *Swift* afterglows (the achromatic behaviour was not robustly established in the pre-*Swift* era). The same conclusion has been reached by Panaitescu et al. (2006), Willingale et al. (2007) and Burrows & Racusin (2007) in independent studies. Alternatively, the funnel opening angle might not be directly linked to the jet opening angle: in other words, the naive expectation $\theta \sim \theta_j$ might be wrong. These reasons drive us to explore the prediction of the reflection model for larger θ. Moreover, in Sect. 5 we showed that the restarted activity of the GRB central engine might be the source of the observed line emission if the ionizing radiation is nearly isotropic and the material intercepts most of the ionizing flux. In that section we also showed that under the assumption that the reprocessing material is the SN shell expanding at $v_{\rm shell} \sim 10^9$ cm s^{-1}, we obtain $\theta \sim 22°$, 17° and 5° for progenitor radii of the order of 10^{11}, 10^{12} and 10^{13} cm, respectively. In this scenario the SN shell expansion began ∼3000 s before the first GRB emission detected by BAT. Consequently, at $t \sim 100$ s we have $R_{\rm o} \sim R_{\rm p} + 3 \times 10^{12}$ cm. With $M_{\rm Ni}^* = 0.4\ M_\odot$, we find that the detected emission requires $T \sim 10^7$ K for $\theta \sim 20°$ (0.3 rad) regardless of the internal radius assumed. No prediction can be made about the stratification index.

In this work we considered an efficiency of production of line photons by the reflection mechanism of the order of 1%. However, the line production efficiency is a strong function of the ionization parameter (Lazzati et al. 2002) ξ, here defined as:

$$\xi = \frac{4\pi D_{\rm L}^2 F_{[1-10]}}{R^2 n} \quad (19)$$

where F_{1-10} is the 1−10 keV ionizing flux; $D_{\rm L}$ is the luminosity distance (∼4150 Mpc for $z = 0.703$); R is the distance of the reprocessing material and n is the particle density. The last column of Table 2 lists the quantity nR^2 for $\xi = 10^4$; the 1−10 keV luminosity is derived from the XRT light curve. For a total shell mass of 10 $M_\odot$ (order of magnitude of the stimated mass ejected by HNe explosion, see e.g. Iwamoto et al. 1998; Mazzali et al. 2003; Mazzali et al. 2006b; Mazzali et al. 2006a) and a scale distance $R \sim 10^{12}$ cm (∼ $v_{\rm shell} \times t_{\rm SN}$) we obtain $nR^2 \approx 10^{45}$ cm^{-1},a value we actually derive from the observed XRT luminosity between 100 and 130 s for $\xi = 10^4$. At this very high value of the ionization parameter, Ni line production efficiencies ≈1% can be obtained only for higher than solar metallicities (Lazzati et al. 2002). In particular, the SN material associated with GRB 060904B must have a metallicity of the order of ten times the solar value.

Finally, GRB jets might be structured, with an angle-dependent energy per solid angle and Lorentz Γ factor as well: power-law jets or Gaussian jets have been proposed recently in

the literature (see e.g. Zhang & Mészáros 2002). Unfortunately, the jet angular structure is still unknown: for this reason no assumption has been made about the angular distribution of the jet energy. As a consequence, our results have been calculated assuming that the detected radiation is representative of the whole emitted radiation, regardless of the direction of emission. However, in the most realistic situation the emission properties of the ionizing continuum are likely to change with θ.

8. Summary and conclusions

M07 recently reported the detection of a spectral feature in excess of the standard single power law behaviour in GRB 060904B spectra. The emission was detected $\approx 10^2$ s after the onset of the GRB, lasted more than 47 s with an isotropic luminosity of $\approx 10^{47}$ erg s^{-1} (three orders of magnitude higher than previously claimed detections). From the spectroscopic point of view, the detected feature can be interpreted as He-like or H-like Ni emission. Given the poor statistics it is not possible to discuss the line profile.

The peculiarity of the detection motivated us to explore in detail the theoretical implications of the presence of highly ionised Ni emitting $\approx 10^2$ s after the burst. Given the typical $\tau_T \gg 1$ (Sect. 3) only reflection models have been considered. Within these models, the external reflection scenario fails to predict the observed luminosity when standard values of the wind velocity and mass loss rate of the progenitor star are used. On the other hand, *if* this is Ni line emission, the detected feature can be interpreted in a funnel scenario with the line produced in reflection and typical Ni masses of the order of 0.1 $M_\odot$ for $\theta = \theta_j \sim 5°$, $T \sim 10^6$ K. Such high values of Ni masses strongly suggest the presence of a SN explosion associated with the GRB event. Alternatively, *if* the reprocessing material is provided by the SN shell and *if* the giant X-ray flare that dominates the early XRT light curve is the ionizing source, the expansion of the SN shell began $\approx$3000 s before the GRB detection, $M^*_{Ni} \sim 0.4\ M_\odot$, $\theta \sim 20°$ and $T \sim 10^7$ K. These models imply mean electron densities $n_e \sim 10^{21}$ cm^{-3} for ten times solar metallicity ($X \sim 10^{-2}$).

Starting from simple analytical models, we presented a consistent scenario in which the line emission can in principle arise. Given the importance of the claim, the subject calls for further study.

Acknowledgements. This work is supported by OAB-INAF by ASI grant I/011/07/0, by the Ministry of University and Research of Italy (PRIN 2005025417) and by the University of Milano Bicocca (Italy).

References

Amati, L. 2006, MNRAS, 372, 233
Arnett, D. 1996, in Supernova & Nucleosynthesis, ed. J. P. Ostriker (Princeton University Press)
Band, D., Matteson, J., Ford, L., et al. 1993, ApJ, 413, 281
Blondin, J. M., & Ellison, D. C. 2001, ApJ, 560, 244
Böttcher, M. 2004, Adv. Space Res., 34, 2696
Burrows, D. N., & Racusin, J. 2007, ArXiv Astrophysics e-prints
Butler, N. R. 2007, ApJ, 656, 1001
Campana, S., Mangano, V., Blustin, A. J., et al. 2006, Nature, 442, 1008
Covino, S., Malesani, D., Tagliaferri, G., et al. 2006, ArXiv Astrophysics e-prints
Dickey, J. M., & Lockman, F. J. 1990, ARA&A, 28, 215
Fugazza, D., D'Avanzo, P., Malesani, D., et al. 2006, 5513, 1
Galama, T. J., Vreeswijk, P. M., van Paradijs, J., et al. 1998, Nature, 395, 670
Ghisellini, G., Lazzati, D., Rossi, E., & Rees, M. J. 2002, A&A, 389, L33
Iwamoto, K., Mazzali, P. A., Nomoto, K., et al. 1998, Nature, 395, 672
Kobayashi, S., & Sari, R. 2001, ApJ, 551, 934
Kobayashi, S., Piran, T., & Sari, R. 1997, ApJ, 490, 92
Lamb, D. Q., Donaghy, T. Q., & Graziani, C. 2005, ApJ, 620, 355
Lazzati, D. 2000, Ph.D. Thesis
Lazzati, D., Ramirez-Ruiz, E., & Rees, M. J. 2002, ApJ, 572, L57
Malesani, D., Tagliaferri, G., Chincarini, G., et al. 2004, ApJ, 609, L5
Markwardt, C., Barbier, L., Barthelmy, S. D., et al. 2006, 5520, 1
Mazzali, P. A., Deng, J., Tominaga, N., et al. 2003, ApJ, 599, L95
Mazzali, P. A., Deng, J., Nomoto, K., et al. 2006a, Nature, 442, 1018
Mazzali, P. A., Deng, J., Pian, E., et al. 2006b, ApJ, 645, 1323
Moretti, A., Margutti, R., Pasotti, F., & Chincarini, G. 2007, A&A, submitted
O'Brien, P. T., Willingale, R., Osborne, J., et al. 2006, ApJ, 647, 1213
Panaitescu, A., Mészáros, P., Burrows, D., et al. 2006, MNRAS, 369, 2059
Patat, F., Cappellaro, E., Danziger, J., et al. 2001, ApJ, 555, 900
Piran, T. 2005, Rev. Mod. Phys., 76, 1143
Protassov, R., van Dyk, D. A., Connors, A., Kashyap, V. L., & Siemiginowska, A. 2002, ApJ, 571, 545
Sako, M., Harrison, F. A., & Rutledge, R. E. 2005, ApJ, 623, 973
Stanek, K. Z., Matheson, T., Garnavich, P. M., et al. 2003, ApJ, 591, L17
Sunyaev, R. A., & Titarchuk, L. G. 1980, A&A, 86, 121
Verner, D. A., & Ferland, G. J. 1996, ApJS, 103, 467
Verner, D. A., & Yakovlev, D. G. 1995, A&AS, 109, 125
Vietri, M., Ghisellini, G., Lazzati, D., Fiore, F., & Stella, L. 2001, ApJ, 550, L43
Willingale, R., O'Brien, P. T., Osborne, J. P., et al. 2007, ApJ, 662, 1093
Woosley, S. E., & Weaver, T. A. 1995, ApJS, 101, 181
Zhang, B., & Mészáros, P. 2002, ApJ, 571, 876
Zhang, B., & Mészáros, P. 2004, Int. J. Mod. Phys. A, 19, 2385
Zhang, B., Dai, X., Lloyd-Ronning, N. M., & Mészáros, P. 2004, ApJ, 601, L119
Zhang, B., Liang, E., Page, K. L., et al. 2007a, ApJ, 655, 989
Zhang, B., Zhang, B.-B., Liang, E.-W., et al. 2007b, ApJ, 655, L25